ELSEVIER

Available online at www.sciencedirect.com

SCIENCE DIRECT®

Journal of Magnetism and Magnetic Materials 293 (2005) 892–902

Journal of magnetism and magnetic materials

www.elsevier.com/locate/jmmm

Influence of the phase separation effect on low-field magnetic properties of $La_{1-x}Ba_xMnO_3$

R. Laiho[a], K.G. Lisunov[a,b], E. Lähderanta[a,c,*], V.S. Zakhvalinskii[a,d], V.L. Kozhevnikov[e], I.A. Leonidov[e], E.B. Mitberg[e], M.V. Patrakeev[e]

[a] *Wihuri Physical Laboratory, Department of Physics, University of Turku, FIN-20014 Turku, Finland*
[b] *Institute of Applied Physics, Academiei Str. 5, MD-2028 Kishinev, Moldova*
[c] *Department of Physics, Lappeenranta University of Technology, P.O. Box 20, FIN-53851 Lappeenranta, Finland*
[d] *Belgorod State University, Pobeda Str. 85, 308015 Belgorod, Russia*
[e] *Institute of Solid State Chemistry, GSP 14591 Pervomaiskaia, 620219 Ekaterinburg, Russia*

Received 9 August 2004; received in revised form 2 December 2004
Available online 4 January 2005

Abstract

Magnetic susceptibility, $\chi(T)$, is investigated in ceramic $La_{1-x}Ba_xMnO_3$ (LBMO) with $x = 0.02-0.25$ in the range of fields $B = 10-80$ G and temperatures $T = 5-310$ K. All samples exhibit a paramagnetic (PM) to ferromagnetic (FM) transition with T_C increasing with x from 177 K ($x = 0.02$) to 295 K ($x = 0.25$) and magnetic irreversibility decreasing below T_C with increasing x. In the PM phase an interval of the Curie–Weiss behavior of $\chi(T)$ with an effective Bohr magneton number, $p_{eff} \sim 30-40$, is observed above $T_1 \sim 260-290$ K. Below T_1 and down to $T_{cr} \sim 190-220$ K the susceptibility follows the scaling law $\chi^{-1}(T) - \chi^{-1}(T_C) \sim (T/T_C - 1)^{\gamma}$ with $\gamma = \gamma_1 \approx 1.4$ corresponding to a three-dimensional (3D) Heisenberg spin system. Below T_{cr}, $\chi(T)$ obeys the same scaling law as for $T > T_{cr}$, but with another value of $\gamma = \gamma_2 \approx 1.7-1.8$, characteristic of a 3D percolation system. The temperature dependence of the susceptibility observed in the PM phase is explained by small FM particles embedded in the host LBMO matrix above T_1. The size of these particles increases between T_1 and T_{cr} up to nanometer scale, forming critical percolation clusters below T_{cr}. The magnetic irreversibility is connected to a mixed, FM and cluster-glass, phase.

PACS: 75.30.Kz; 75.40.Cx; 75.30.Vn

Keywords: Magnetic phase boundaries; Critical exponents; Magnetic clusters

1. Introduction

$La_{1-x}Ba_xMnO_3$ (LBMO) belongs to hole-doped mixed-valence manganite perovskites, exhibiting a

*Corresponding author. Wihuri Physical Laboratory, Department of Physics, University of Turku, FIN-20014 Turku, Finland. Tel.: +358 405545227; fax: +358 22319836.
E-mail address: erlah@utu.fi (E. Lähderanta).

0304-8853/$ - see front matter © 2004 Elsevier B.V. All rights reserved.
doi:10.1016/j.jmmm.2004.12.021

colossal magnetoresistance (CMR) effect accompanied with a metal–insulator transition (MIT) [1]. These compounds also have a rich magnetic phase diagram, including high-temperature paramagnetic (PM), ferromagnetic (FM), antiferromagnetic (AF) [2] and glassy behavior [3,4]. Hole-doping of the manganites by substitution of a divalent alkaline element for La^{3+} or formation of cation vacancies introduces, besides Mn^{3+}, a fraction c of Mn^{4+} leading to FM Mn^{3+}–Mn^{4+} double exchange interaction competing with AFM Mn^{3+}–Mn^{3+} superexchange interaction. This model was used to interpret the origin of the spin-ordered phases in the early period of investigations [5]. On the other hand, further extensive work has demonstrated that the picture of competing SE–DE interactions alone cannot explain the full set of electronic and magnetic properties of the manganite perovskites. Namely, the elements of the magnetic phase diagram corresponding to the charge and/or orbital ordering and those with coexistence of the different magnetic phases, the CMR effect, the MIT and even the shape of the resistivity vs. temperature plots depending on the doping level are found to be incompatible with a simple picture of the electronically homogeneous material, suggesting an important role of the phase separation in the manganites [6].

Evidence of the coexistence of different electronic (metallic and insulating) and magnetic (FM and AFM or PM) as well as charge and/or orbitally ordered phases in manganites is obtained by a vast number of investigations, both experimental and theoretical. Namely, the relevance of the phase separation was confirmed by various macroscopic (resistivity and magnetoresistance, magnetization, Hall effect), and microscopic (electron microscopy, scanning tunneling spectroscopy, neutron diffraction, elastic and small-angle scattering, muon spin relaxation, and Mössbauer spectroscopy) investigations in conventional hole-doped manganites as $La_{1-x}Ca_xMnO_3$ [7–10] and $La_{1-x}Sr_xMnO_3$ [11,12] within a broad range of composition. Phase separation has been observed in $La_{5/8-y}Pr_yCa_{3/8}MnO_3$ ($y = 0-0.42$) [13], $(La_{1-x}Tb_x)_{2/3}Ca_{1/3}MnO_3$ ($x = 0-1$) [14], $(La_{0.25}Nd_{0.75})_{0.7}Ca_{0.3}MnO_3$ [15], $(La_{0.5}Nd_{0.5})_{2/3}Ca_{1/3}MnO_3$ [16], $Pr_{1-x}Sr_xMnO_3$ and $Nd_{1-x}Sr_xMnO_3$ [17], as well as in the electron-doped and layered perovskites and pyrochlores (for references see [6]). This implies that phase separation is an intrinsic property of the manganites, which is not connected to the chemical composition and inhomogeneity or preparation details. This statement was reproduced in extensive theoretical investigations [6] associating the phase separation with instability like a discontinuity of the density of mobile e_g electrons vs. the chemical potential [18] accompanied by charge constraints (breaking of the macroscopic regions of different phases into a mixture of nanosize regions due to the long-range Coulomb interactions) [19]. Parametric phase diagrams containing coexisting phases were obtained using a broad series of approximations in the model Hamiltonian, e.g. one- or two-orbital models with or without the Jahn–Teller effect or Coulomb correlations, under a wide variation of the values of the Hund coupling constant and the transfer integral and for various dimensionalities of the system (for details see [6] and references therein).

Among other CMR compounds, up to now the manganites doped with Ca or Sr have been investigated most extensively [2,6]. However, in comparison with e.g. $La_{1-x}Ca_xMnO_3$ a change in the hole-doping method can lead in its close analog, cation-deficient $LaMnO_{3+\delta}$, to a series of new effects due to stronger structural changes caused by the doping [20].

Low-field ($B \sim 1-100$ G) investigations of the macroscopic magnetization with minimal perturbation of the spin system have yielded important microscopic information about $La_{1-x}Ca_xMnO_3$ and $LaMnO_{3+\delta}$ [4,20]. In this paper, we extend our investigations to the microscopic state of LBMO, which shows high sensitivity to the doping level [21,22].

2. Experimental results and analysis

2.1. Experimental details

LBMO samples with $x = 0.02-0.35$ (marked below as S02, S04 etc, with the numerical

part equal to $100x$) were synthesized with the conventional solid-state reaction method from La_2O_3, Mn_3O_4 and $BaCO_3$. The raw materials were pre-calcined to remove possible adsorbates, weighed in stoichiometric proportions and mixed with addition of ethanol. The mixtures were pressed into pellets and fired at 900–1300 °C in air, crushed into powder, pressed and fired several times with gradually increasing the temperature until a single-phase material was obtained. The phase purity and the lattice structure were determined with room-temperature X-ray powder diffraction investigations ($\lambda = 1.54178$ Å), establishing the rhombohedral *R-3c* ($x = 0.02-0.2$) and the orthorhombic *Imma* ($x = 0.25-0.35$) space groups of the samples. The values of the lattice parameters a, b and c agree closely with those published in [23].

Temperature dependence of the DC magnetization, $M(T)$, was determined with an RF-SQUID magnetometer after cooling the samples from the room temperature down to 5 K in zero field (ZFC) or in a field (FC) of $B = 10$ G (S02–S10) and 80 G (S15–S25). The temperature dependence of the thermoremanent magnetization (TRM) was measured after cooling the samples from the room temperature down to 5 K in the field of 10 G (S02–S10) or 80 G (S15–S25) and then reducing the field to zero. The dependences of $\chi_{ZFC}(T)$ and $\chi_{FC}(T)$ (where $\chi = M/B$) are shown in Fig. 1.

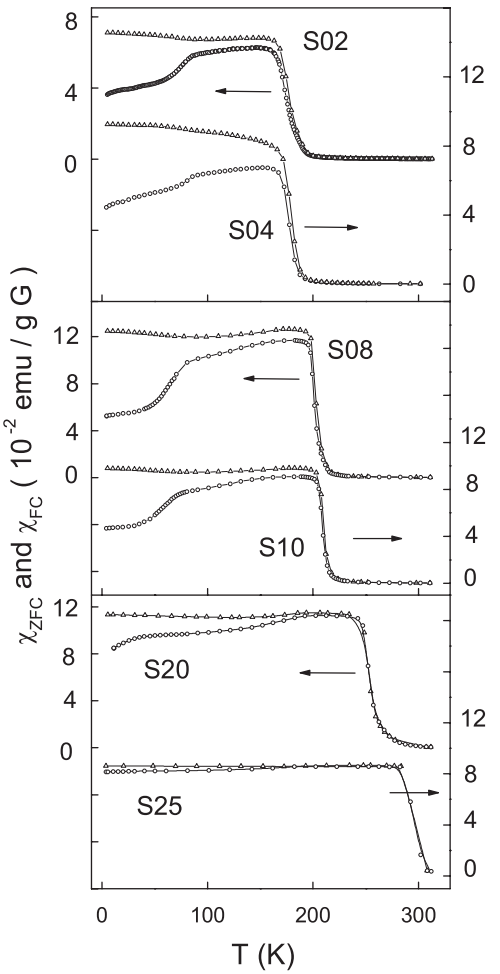

Fig. 1. Temperature dependences of χ_{ZFC} (○) and χ_{FC} (△) in the LBMO samples.

2.2. Dependence of the PM–FM transition temperature on Ba concentration

Both $\chi_{ZFC}(T)$ and $\chi_{FC}(T)$ exhibit in all the samples a PM−FM transition at a Curie temperature T_C, determined from the inflection point of the corresponding interpolation curves. As can be seen in Fig. 2, the value of T_C increases with x. However, in the manganite perovskites the PM−FM transition takes place at values of c above ~0.15–0.20 [2] definitely larger than x for S02–S10. This difference points out that both ways of the hole doping, substitution of Ba^{2+} for La^{3+} and creation of cation vacancies, should be taken into account. In such case x and c are connected through the equation

$$c(x) = \frac{x^2 + \delta x + 3\delta^2}{x + \delta}, \tag{1}$$

where δ is the concentration of the cation vacancies introduced in the lattice during preparation of the sample [3]. To analyze the dependence of $T_C(x)$ we apply the model of Varma [24],

$$kT_C \approx 0.05 Wc(1 - c), \tag{2}$$

which treats the PM−FM transition of the manganites by considering the magnetic disorder

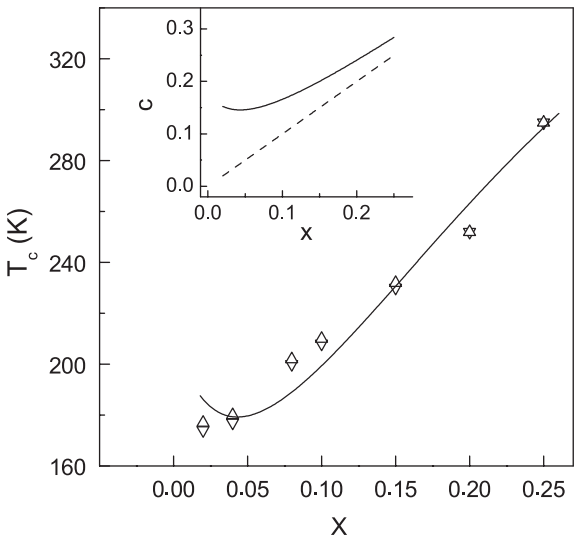

Fig. 2. Dependence of T_C on x for LBMO determined from the inflection points of the interpolated curves of $\chi_{ZFC}(T)$ and $\chi_{FC}(T)$ ($\triangledown$ and $\triangle$, respectively). The solid line is evaluated with Eq. (2) as described in the text. Inset: Dependence of c on x calculated with Eq. (1) (the solid line). The dashed line represents the concentration of Ba^{2+}.

and localization of the electrons inside a band of width W. This model has been used to interpret the transition temperature in various CMR compounds, like $La_{1-x}Sr_xMnO_3$ [24], $La_{1-x}Ca_xMnO_3$ [3], $LaMnO_{3+\delta}$ [20] and $LaMn_{1-x}Ni_xO_3$ [25].

The solid line in Fig. 2 represents the best fit of the experimental values of $T_C(x)$ with Eq. (2). A reasonable agreement is obtained for $W = 2.45 \pm 0.07$ eV and $\delta = 0.059 \pm 0.004$, taking into account that δ is sensitive to details of the preparation method and can vary randomly from sample to sample. The value of W lies between those in $La_{1-x}Sr_xMnO_3$ (2.5 eV) [24] and $La_{1-x}Ca_xMnO_3$ (≈ 1.9 eV) [3], while δ is close to 0.062–0.071 found in $La_{1-x}Ca_xMnO_3$ [3]. As can be seen from the inset in Fig. 2, the function $c(x)$ evaluated with Eq. (1) (the solid line) deviates for small x considerably from x (the dashed line) and tends to the concentration of Ba^{2+} when x is increased, exhibiting the same behavior as in LCMO [3]. Between $x = 0.02$ and 0.1 the dependence of $c \sim 0.15-0.17$ on x is weak.

2.3. Irreversibility phenomena in LBMO

As can be seen in Fig. 1, a magnetic irreversibility or the deviation of $\chi_{ZFC}(T)$ from $\chi_{FC}(T)$, which is weak near T_C and increases as T is decreased below T_C, is observed between $x = 0.02$ and 0.15 (the dependences of χ_{ZFC} and χ_{FC} on T for S15 are similar to those of S10). In S20 the weak irreversibility around T_C vanishes, while with a further increase of x, the deviation of $\chi_{ZFC}(T)$ from $\chi_{FC}(T)$ is strongly suppressed in the whole temperature interval below T_C (bottom panel of Fig. 1). Another feature of the susceptibility curves in Fig. 1 is the weak temperature dependence of $\chi_{ZFC}(T)$ for S02–S10 between T_C and $\sim$80 K followed by the inflection of $\chi_{ZFC}(T)$ at $T_r \sim 70$ K and its rapid decrease around T_r before slowing down below $\sim$60 K. With increasing x this feature is also suppressed.

The irreversible magnetic behavior is an indication of a frustrated magnetic state in LBMO. In frustrated systems the difference between $\chi_{ZFC}(T)$ and $\chi_{FC}(T)$ is governed by spin dynamics and is usually observed below the onset of freezing-in of the ionic magnetic moments in a *spin-glass* (SG) phase, or freezing-in of the moments of the FM clusters in a *cluster-glass* (CG) phase [26]. In SG the frustration is connected to competing interactions between the magnetic moments, while in CG the shape and size distributions of the clusters may also be important [26,27]. These glassy states can be distinguished by comparison of TRM (T) and the difference of the $M_{FC}(T)$ and $M_{ZFC}(T)$ functions [3,27,28]. Namely, in the SG system the equation $M_{FC}(T) - \mathrm{TRM}(T) = M_{ZFC}(T) - 0$, where 0 represents the zero level of the magnetization, is connected to the symmetry of the energy distribution of potential barriers in the presence or absence of a magnetic field. When the system is heated, it can make a transition to a metastable state separated by an energy barrier not exceeding the thermal activation energy and can be expressed by the $M_{ZFC}(T) - 0$ value. When the field is switched on, the SG adopts a certain metastable state $M_{FC}(T, B)$ depending on the temperature and the field and attains after switching off the field a certain value of TRM (T). Hence, in the SG phase

an expression

$$\mathrm{TRM}(T) = M_{\mathrm{FC}}(T) - M_{\mathrm{ZFC}}(T) \quad (3)$$

may be expected, whereas in the CG phase deviations from this behavior may arise due to the anisotropy associated with the shape and orientation of the clusters [27,28].

From Fig. 3 it is obvious that Eq. (3) is generally not satisfied in LBMO with x between 0.02 and 0.1. This condition is fulfilled only roughly well below T_C in S02 and within a limited interval between $T \approx 90-150$ K in S04, whereas in S08 and S10 considerable differences between TRM (T) and $M_{\mathrm{FC}}(T) - M_{\mathrm{ZFC}}(T)$ are observed. Another important feature is a peak of $M_{\mathrm{FC}}(T) - M_{\mathrm{ZFC}}(T)$ at T_C (marked by vertical arrows at average values of T_C, shown for $\chi_{\mathrm{ZFC}}(T)$ and $\chi_{\mathrm{FC}}(T)$ in Fig. 2) indicating a qualitative disagreement with Eq. (3). For LCMO [3] (the bottom panel in Fig. 3) a good coincidence of TRM (T) and $M_{\mathrm{FC}}(T) - M_{\mathrm{ZFC}}(T)$ is observed for $x = 0$ (plots 1) and 0.05 (plots 2), where the respective values of $c \approx 0.19$ and 0.15 are comparable with $c \approx 0.15-0.17$ for the samples S02–S10. Distinct deviations from Eq. (3) are observed in LCMO for $x = 0.15$ and $c \approx 0.20$ (plots 3). With further increase of x and c the magnetic behavior of LCMO displays larger deviations from Eq. (3), demonstrating a gradual transition from the SG to the CG phase [3]. However, no peaks of $M_{\mathrm{FC}}(T)$–$M_{\mathrm{ZFC}}(T)$ curves near T_C were observed in this compound up to $x \approx c \approx 0.4$ [3].

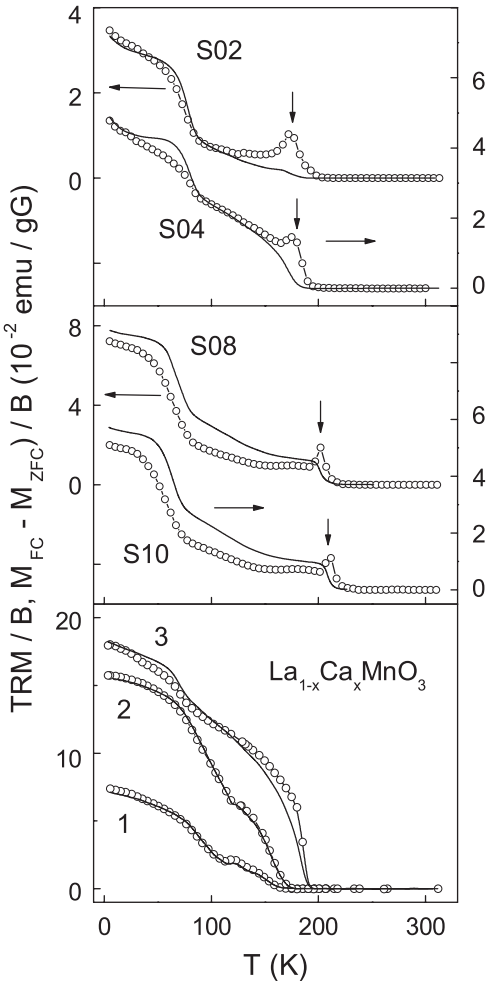

Fig. 3. Temperature dependence of TRM/B (solid lines) and $(M_{\mathrm{FC}} - M_{\mathrm{ZFC}})/B$ (symbols) for the LBMO samples S02–S10 (upper and middle panels) and for LCMO (lower panel) with $x = 0$ and $c \approx 0.19$ (plots 1), $x = 0.05$ and $c \approx 0.15$ (plots 2) and $x = 0.15$ and $c \approx 0.20$ (plots 3) [4]. The arrows mark the average values of T_C, determined from $\chi_{\mathrm{ZFC}}(T)$ and $\chi_{\mathrm{FC}}(T)$, in Fig. 2.

2.4. Temperature dependence of the susceptibility above T_C

We restrict the analysis of the PM phase in LBMO with x between 0.02 and 0.10, having T_C well below the room temperature. This allows us to investigate a sufficiently wide temperature interval to discuss the magnetic behavior of the samples above T_C in detail.

In the temperature interval of $T > T_1$ well above T_C, where the short-range FM fluctuations are negligible, the susceptibility is expected to follow the Curie–Weiss law, $\chi(T) = C/(T - \theta)$, where $C = p_{\mathrm{eff}}^2 \mu_B^2 N/(3k)$, p_{eff} is the effective Bohr magneton number per magnetic ion, N is the concentration of the magnetic ions and θ is the Weiss temperature. As can be seen from Fig. 4 the plots of $\chi^{-1}(T)$ vs. T can be fitted to the Curie–Weiss law, above $T_1 \approx 260$ K for S02 and S04, $T_1 \approx 280$ K for S08 and $T_1 \approx 290$ K for S10, yielding $p_{\mathrm{eff}}^2 \approx 35$, 34, 40 and 33 for S02, S04, S08 and S10, respectively, if N is taken equal to the Mn concentration $1.3 \times 10^{22}\,\mathrm{cm}^{-3}$. These values of p_{eff}^2 exceed that of $p_{\mathrm{eff}}^2 \approx 22$, expected for a mixture

of Mn^{3+} and Mn^{4+} given by the ratio $c \sim 0.15-0.17$ above, where the Mn ion spin is taken as a weighted mean value between those of Mn^{3+} ($S = 2$) and Mn^{4+} ($S = \frac{3}{2}$).

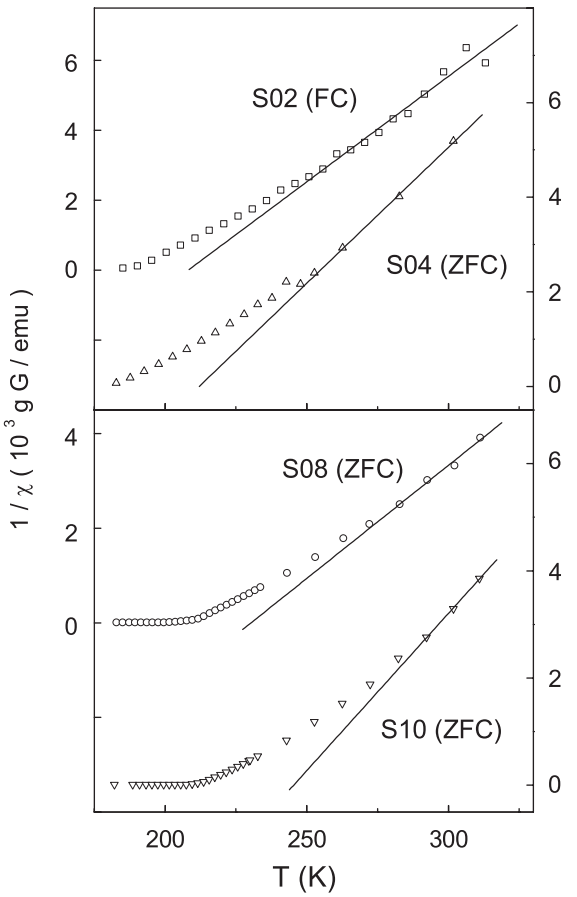

Fig. 4. Temperature dependence of the inverse susceptibility measured in the ZFC and FC regimes. The solid lines represent linear fits.

As can be seen from Fig. 4, the Curie–Weiss law is violated with lowering of the temperature. This is attributable to the onset of critical behavior when T approaches T_C from above according to the scaling law, $\chi(T) \sim (T/T_C - 1)^{\gamma}$, where γ is the critical exponent depending on the nature and the dimensionality of the spin system [29]. For analysing the experimental data, it is convenient to write

$$\chi^{-1} - \chi_C^{-1} \sim \tau^{\gamma}, \tag{4}$$

where $\chi_C = \chi(T_C)$ and $\tau = T/T_C - 1$. The dependences of $\ln(\chi^{-1}-\chi_C^{-1})$ on $\ln\tau$ are plotted by interpolation of $\chi(T)$ and the variation of T_C around the values obtained above (Fig. 2) with a step of 0.5 K, to achieve the minimum standard deviation of the linear fits to the experimental data with Eq. (4). As can be seen from Table 1, the values of T_C specified in this way ($T_C^{(s)}$), coincide with those obtained from the inflection points of the interpolation curves ($T_C^{(i)}$) for S04 and S10, while the deviations for S02 and S08 are ~4% and ~1%, respectively, which suggests somewhat higher macroscopic inhomogeneity of these samples.

The plots of $\ln(\chi^{-1}-\chi_C^{-1})$ vs. $\ln\tau$ for S02–S10 are shown in Fig. 5. For all samples, independent of the cooling conditions (ZFC or FC) these plots contain (below a crossover temperature T_{cr}) a linear part with the same slope γ_1. The values of γ_1 and T_{cr} are collected in Table 1. In addition to the low-temperature slope, in Fig. 5, a broad linear interval can be seen between T_{cr} and T_1 (marked with arrow) with the same slope for all samples and the critical exponent γ_2 (see Table 1). In Fig. 5 one can also see a broad intermediate interval between the two linear parts of the plots for S02 and a similar, but less pronounced, between the

Table 1
Values of the temperatures $T_C^{(i)}$ obtained from inflection points of the interpolated curves of the susceptibility and $T_C^{(s)}$ specified by fitting the susceptibility to the scaling law, the critical exponents γ_1 and γ_2 and the crossover temperature T_{cr} for the $La_{1-x}Ba_xMnO_3$ samples in the ZFC and FC cooling regimes

Sample no.	Regime	$T_C^{(i)}$ (K)	$T_C^{(s)}$ (K)	γ_1	γ_2	T_{cr} (K)
S02	ZFC	174	166.5	1.76±0.03	1.44±0.04	192
S04	FC	180	180	1.75±0.02	1.38±0.02	195
S08	ZFC	200	198.5	1.75±0.05	1.38±0.02	215
S10	ZFC	208	208	1.77±0.04	1.37±0.02	220

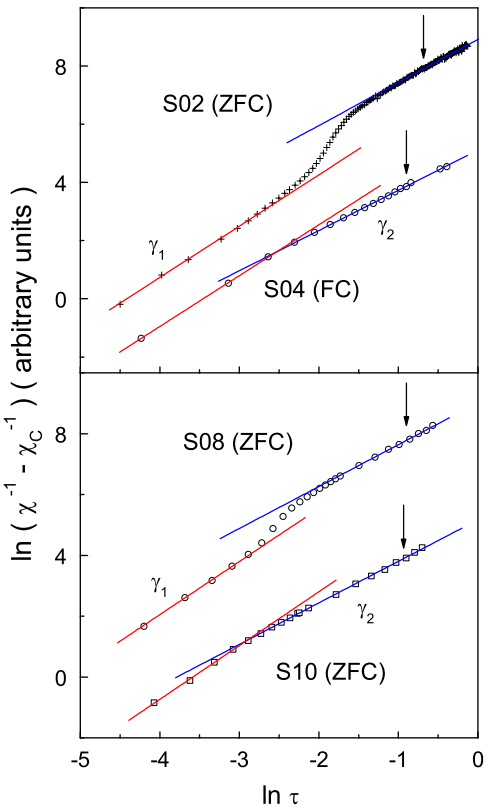

Fig. 5. The plots of $\ln(\chi^{-1}-\chi_C^{-1})$ vs. $\ln\tau$ for the samples S02–S10 in different cooling regimes, corresponding to the 3D percolation system with $\gamma_1 \approx \gamma_p$ and the 3D Heisenberg system with $\gamma \approx \gamma_H$. The arrows mark the temperature T_1. The solid lines represent linear fits.

linear parts with different slopes for S08. Such intermediate regions are not found in S04 and S10. Taking into account the differences between the values of T_C in S02 and S08 (Table 1), this behavior is consistent with macroscopic inhomogeneity of S02 and S08.

3. Discussion

3.1. Introductory remarks

As mentioned above (Section 1) the broad set of the electronic and magnetic phenomena in the manganites is governed by the phase separation, which is the intrinsic property of these materials. Below, we discuss briefly some related features of the phase separation effect important for interpretation of the low-field magnetization data in LBMO.

The key property established both theoretically and experimentally, is the percolative picture of the coexisting phases [7,10,13,14]. At this point it is worth mentioning the interesting numerical investigations simulating the effect of the percolative phases in the manganites by the random field Ising model [30]. A percolative system near the transition (e.g. MIT) is quite sensitive to an external influence, so that only a small agitation could push it towards the transition (generation of the infinite cluster), which drastically changes its properties [6,31]. Such a behavior is in line with a vast number of experimental investigations, including the CMR effect itself (see [6] and references therein).

Another important property of the phase separation effect is the sensitivity of the coexisting phase ratio (e.g. the metal/insulator or the PM/FM fraction) to the temperature and the applied magnetic field. Experimentally this was observed in [8,9], whereas a similar conclusion was drawn by modeling the resistivity plots parameterized by the field in the semi-phenomenological approach based on the Miller-Abrahams random resistivity network [32]. Namely, the fraction of the FM (metallic) phase has been found to increase as B is increased or T is decreased approaching T_C. Generally, existence of a new temperature scale in the manganites, T^*, connected to the onset of the phase separation upon cooling has been proposed [6].

A property of the phase separation in the manganites also worth mentioning is its strong sensitivity to the lattice (or chemical) disorder, which means that the random substitution of a trivalent A element (e.g. La^{3+}) for a divalent A′ element (e.g. Ca^{2+}) suggests a random distribution of the strength of both the FM and AF interactions within some intervals, connected not only to the difference of the ionic radii r_A and $r_{A'}$, but also to the variance $\sigma^2 = \langle r_A^2\rangle - \langle r_A\rangle^2$, where $\langle r_A\rangle = (1-x)r_A + xr_{A'}$ etc. [6,33]. It has been shown that the strong disorder of this type induces breaking of the large coexisting clusters into

smaller ones, whereas even a small but nonzero disorder can stimulate generation of a percolative system with very large clusters [6,30]. In addition, such disorder can act as a smoothing factor of the first-order phase transition between strongly different phases for e.g. FM and AF ones, setting in the percolative transition between them [15–17,30]. Experimentally, the micrometer size coexisting clusters, not connected to the extrinsic effects but related to disorder, have been observed in $La_{5/8-y}Pr_yCa_{3/8}MnO_3$ [13].

3.2. Magnetic properties above T_C

The enhanced value of p_{eff} found in the Curie–Weiss region is attributable to generation of small FM clusters in the PM background already at $T > T_1$, so that the scale T^* defined in [6] can be ascribed to temperatures well-above T_C, exceeding even the room temperature. This is in line with the investigations of the Hall effect in $La_{0.7}Ca_{0.3}MnO_3$ where the existence of a two-phase state was found below $1.4T_C$ [10], and with recent investigations of the resistivity relaxation in $La_{0.8}Ca_{0.2}MnO_3$ yielding $T^* \sim 350$ K [34].

Until the FM clusters are sufficiently small the spin system is expected to satisfy conditions of the 3D Heisenberg universality class, characterized by the value of the critical exponent $\gamma_H = 1.39$ [29,35], which is close to γ_2 in Table 1. Similar values of $\gamma = 1.39-1.43$ in $La_{1-x}Sr_xCoO_3$ [36], $\gamma = 1.39 \pm 0.05$ in $La_{0.95}Mg_{0.05}MnO_3$ [37] and $\gamma = 1.45$ in $La_{0.8}Ca_{0.2}MnO_3$ [38] have been reported earlier.

A transformation of an assembly of small weakly correlated independent carriers of the magnetic moments into the strongly correlated percolative system of large FM clusters by increasing the cluster radius r and the volume fraction of the FM phase $\eta(r)$ with lowering the temperature may change the critical behavior of $\chi(T)$. This would set in when the correlation length $\lambda \approx R\tau^{-\nu}$ [39], where $R \approx 2(4\pi n/3)^{-1/3}$ is the mean distance between the FM particles, n is their concentration and $\nu \approx 1$ is the critical exponent of λ, becomes much longer than the lattice parameter, yielding the scaling behavior of $\chi(T)$ according to Eq. (4) with the critical exponent $\gamma = \gamma_p$. The values of $\gamma_p = 1.69 \pm 0.05$ [40], 1.70 ± 0.11 [41] and 1.80 ± 0.05 [42] of a 3D percolation system, evaluated numerically, are close to γ_1 in Table 1.

As follows from the consideration above, at T_{cr} the FM particles can be treated roughly as a system of uncorrelated magnetic moments having a predominant contribution to $M(T_{cr})$. Therefore, we can express the magnetization approximately as $M(T_{cr}) \approx \mu n L(\mu B/kT_{cr})$, where μ is the moment of the FM particle and $L(\xi)$ is the Langevin function, which for $\xi \ll 1$ gives $\chi(T_{cr}) \approx \mu^2 n/(3kT_{cr})$. The volume fraction of the particles satisfies the equation $\eta \approx \mu n/M_s$, where M_s is the saturation magnetization. From the above expressions we obtain:

$$\mu \approx 3kT_{cr}\chi(T_{cr})/M_s\eta \tag{5}$$

and

$$n \approx \eta^2 M_s^2/[3kT_{cr}\chi(T_{cr})]. \tag{6}$$

If r_c is the critical value of r corresponding to the percolation threshold, τ can be given in the form $\tau = r_c/r - 1$. Then, taking into account that the volume fraction satisfies the equation

$$\eta = 1 - \exp(-4\pi n r^3/3) \tag{7}$$

and that $\eta_c = \eta(r_c) \approx 0.29$ [39], we obtain

$$\eta = 1 - (1 - \eta_c)^{1/(1+\tau)^3}. \tag{8}$$

With Eqs. (5)–(8) we estimate $r \approx 2-3$ nm, $\mu \approx (1-2) \times 10^3\,\mu_B$, $n \approx (5-10) \times 10^{18}\,cm^{-3}$, $\eta \approx 0.20-0.25$ and $\lambda/R_0 \approx 100-200$ (where R_0 is the average distance between the Mn ions), using the values of $\chi(T_{cr}) \approx (3-6) \times 10^{-3}$ emu/g G observed in the samples S02–S10. The results obtained for different samples are similar and do not exhibit a systematic dependence on x. The values of r correspond to nanoscale FM particles, those of λ/R_0 and η are large enough for the onset of the critical percolation behavior at T_{cr}, and μ reaches ~90% of the value corresponding to a fully saturated system of spins within the volume of a particle having the radius r. The values of n given above are similar to $n = 2.1 \times 10^{19}\,cm^{-3}$ observed in $La_{1-x}Ca_xMnO_3$ with $x = 0.05$ and 0.08 by neutron scattering experiments [43] and that of $r \approx 2-3$ nm is close to 5 nm obtained in $La_{0.8}Ca_{0.2}MnO_3$ by Mössbauer investigations at T just below T_C [44].

Hence, the magnetic behavior of LBMO above T_C is consistent with the picture of the phase separation in the manganites discussed in Section 3.1, namely coexisting PM and FM phases with growing volume fraction of the latter to form a percolative magnetic system when T is decreased.

In ceramic $La_{1-x}Ca_xMnO_3$ the critical behavior of $\chi(T)$ in low fields has been found to satisfy Eq. (4), but with different values of γ within two different intervals of x and c, correlating with a transition from the SG to the CG phase below T_C [3]. Namely, it has been established that for $x<0.18$ and $c<0.23$ in different $La_{1-x}Ca_xMnO_3$ samples γ lies between $\gamma_H = 1.39$ [29,36] and the mean-field value $\gamma_{mf} = 1$, while for $0.18<x\leqslant 0.4$ ($0.23<c\leqslant 0.43$) $\gamma \sim 1.6-1.8$, i.e. near γ_p [40–42].

The non-universal critical behavior, characterized by the 3D Heisenberg value of $\gamma \approx 1.37-1.38$ and by the 2D percolation value of $\gamma \approx 2.4$ was observed by us recently in $La_{0.7}Ca_{0.3}MnO_3$ thin films [45]. Existence of two 3D critical regimes of the magnetic susceptibility in different temperature intervals, corresponding to the Heisenberg and the percolation spin systems, was established in ceramic $La_{0.7}Ca_{0.3}Mn_{1-y}Fe_yO_3$ [46], yielding the values of r, μ and n close to those found in the present work. However, in those materials the sequence of the two critical regimes is inverted with respect to that in LBMO, which exhibits the percolation and the Heisenberg spin systems for $T<T_{cr}$ and $T>T_{cr}$, respectively. One of the possible reasons to such a difference may be a different structure of the Ca-doped (orthorhombic *Pnma*) and the Ba-doped compounds. However, another reason, connected to a concentration of $Mn^{4+}\sim 2$ times higher than in S02–S10, seems more likely. Indeed, the enhanced Mn^{4+} concentration may induce the onset of the phase separation effect at higher temperatures. On the other hand, the higher temperature would correspond also to the onset of the charge ordering, which may destroy percolation clusters and restore the Heisenberg spin system with lowering T. In addition, as mentioned in Section 3.2 an important role in the phase separation plays the lattice disorder, which is enhanced in the compounds with higher doping level and may lead in $La_{0.7}Ca_{0.3}Mn_{1-y}Fe_yO_3$ [46] and $La_{0.7}Ca_{0.3}MnO_3$ [45] to percolative clusters within a reduced temperature interval. It is difficult to make a final conclusion at this point, based only on the present data, without more detailed investigations of LBMO with $x>0.2$ in an interval extending well above the room temperature.

3.3. Low-temperature features of the susceptibility

The magnetic irreversibility below T_C (Section 2.3) indicates existence of a frustrated magnetic ground state in LBMO. The percolative PM–FM transition characterized by γ_p means generation of the infinite FM cluster as T approaches T_C from above, which, however, may coexist with finite FM clusters because the critical value of $\eta_c \approx 0.29$ does not suggest that all the material should enter the infinite cluster. This can explain coexistence of the FM and glassy behavior at $T<T_C$ in the samples S02–S10 in conditions of the violation of Eq. (3) (Fig. 3) by existence of a mixed, FM and CG, phase down to T_r. The feature of $\chi_{ZFC}(T)$ at T_r was observed also in $La_{1-x}Ca_xMnO_3$ and interpreted by the *onset of the charge and/or orbital ordering* at $x_{co} = \frac{1}{8}$ [47] or by *transition to a re-entrant glassy state* [4]. It can be seen that despite the values of x in S02–S10 differ from x_{co}, the values of $c \sim 0.15-0.17$ in these samples (Fig. 2) are rather close to x_{co} and neither of the above reasons can be excluded. Moreover, it is reasonable to suppose that even a partial charge ordering would destroy the infinite FM cluster by making the distribution of the holes more homogeneous, so that only the finite FM clusters could exist below T_p. In this case, the two reasons mentioned above would be complementary, thus explaining both the onset of the frequency dependence of the AC susceptibility at T_p [4] and the relatively small fields in which this feature vanishes [47], which are pertinent to the re-entrant glassy transition [26,27], and the value of x_c characterizing the charge and/or orbitally ordered state in the manganites [6,47].

4. Conclusions

We have investigated low-field magnetic properties of ceramic LBMO with $x = 0.02-0.25$. All

samples exhibit a PM–FM transition at T_C increasing with x. The dependence of T_C on x demonstrates that besides substitution of Ba^{2+} for La^{3+}, the hole doping of the material is realized also by generation of cation vacancies, especially for x between 0.02 and 0.10. The magnetic irreversibility observed below T_C reveals the frustrated ground state of LBMO, consisting of the mixed, FM and CG phases. Well above T_C the Curie–Weiss dependence of $\chi(T)$ is observed with values of p_{eff} exceeding that for a mixture of Mn^{3+} and Mn^{4+} ions at a given ratio. Upon lowering the temperature non-uniform scaling behavior of $\chi(T)$, which corresponds to transformation of a high-temperature 3D Heisenberg spin system into a low-temperature 3D percolation spin system is observed. The temperature dependence of the susceptibility observed in the PM phase gives evidence for phase separation due to the generation of nanosize FM clusters and joining them into percolation clusters of a critical size with decrease in temperature. Characteristic parameters of the FM particles are estimated at a crossover of the two critical regimes, demonstrating a reasonable agreement with the literature data for other manganite perovskites.

Acknowledgements

This work was supported by the Wihuri Foundation, Finland, and by INTAS (Project No. INTAS 00-00728).

References

[1] R. von Helmolt, J. Wecker, B. Holzapfel, L. Schulz, K. Sammer, Phys. Rev. Lett. 71 (1993) 2331.
[2] J.M.D. Coey, M. Viret, S. von Molnar, Adv. Phys. 48 (1999) 167.
[3] R. Laiho, K.G. Lisunov, E. Lähderanta, P.A. Petrenko, J. Salminen, V.N. Stamov, V.S. Zakhvalinskii, J. Phys.: Condens. Matter 12 (2000) 5751.
[4] R. Laiho, E. Lähderanta, J. Salminen, K.G. Lisunov, V.S. Zakhvalinskii, Phys. Rev. B 63 (2001) 094405.
[5] P.-G. de Gennes, Phys. Rev. 118 (1960) 141; K. Kubo, N. Ohata, J. Phys. Soc. Japan 33 (1972) 21.
[6] E. Dagotto, T. Hotta, A. Moreo, Phys. Rep. 344 (2001) 1.
[7] M. Fäth, S. Freisem, A.A. Menovsky, Y. Tomioka, J. Aarts, J.A. Mydosh, Science 285 (1999) 1540.
[8] S.J.L. Billinge, R.G. Di Francesco, G.H. Kwei, J.J. Neumeier, J.D. Thompson, Phys. Rev. Lett. 77 (1996) 715.
[9] S.J.L. Billinge, Th. Proffen, V. Petkov, J.L. Sarrao, S. Kycia, Phys. Rev. B 62 (2000) 1203.
[10] S.H. Chun, M.B. Salamon, Y. Tomioka, Y. Tokura, Phys. Rev. B 61 (2000) R9225.
[11] M. Hennion, F. Moussa, G. Biotteau, J. Rodriguez-Carvajal, L. Piusard, A. Revcolevschi, Phys. Rev. B 61 (2000) 9513.
[12] L. Vasiliu-Doloc, J.W. Lynn, A.H. Moudden, A.M. de Leon-Guevara, A. Revcolevschi, Phys. Rev. B 58 (1998) 14 913.
[13] M. Uehara, S. Mori, C.H. Chen, S.-W. Cheong, Nature 399 (1999) 560.
[14] J. Blasco, J. Garcia, J.M. de Teresa, M.R. Ibarra, P.A. Algarabel, C. Marquina, J. Phys.: Condens. Matter 8 (1996) 7427.
[15] J.-S. Zhou, J.B. Goodenough, J.F. Mitchell, Phys. Rev. B 58 (1998) R579.
[16] M.R. Ibarra, G.-M. Zhao, J.M. De Teresa, B. Garcia-Landa, Z. Arnold, C. Marquina, P.A. Algarabel, H. Keller, C. Ritter, Phys. Rev. B 57 (1998) 7446.
[17] J.A. Fernandez-Baca, P. Dai, H.Y. Hwang, C. Kloc, S.-W. Cheong, Phys. Rev. Lett. 80 (1998) 4012.
[18] S. Yunoki, J. Hu, A. Malvezzi, A. Moreo, N. Furukawa, E. Dagotto, Phys. Rev. Lett. 80 (1998) 845; S. Yunoki, A. Moreo, E. Dagotto, Phys. Rev. Lett. 81 (1998) 5612.
[19] E.L. Nagaev, Phys. State Sol. (b) 186 (1994) 9; A. Moreo, S. Yunoki, E. Dagotto, Phys. Rev. Lett. 83 (1999) 2773.
[20] R. Laiho, K.G. Lisunov, E. Lähderanta, P.A. Petrenko, J. Salminen, V.N. Stamov, Yu.P. Stepanov, V.S. Zakhvalinskii, J. Phys. Chem. Solids 64 (2003) 2313.
[21] S.L. Yuan, Y. Jiang, G. Li, Y.P. Yang, X.Y. Zeng, P. Tang, Z. Huang, Phys. Rev. B 61 (2000) 3211.
[22] P. Mandal, Phys. Rev. B 61 (2000) 14 675; P. Mandal, B. Gosh, Phys. Rev. B 68 (2003) 014422.
[23] V.A. Cherepanov, E.A. Filonova, V.I. Voronin, I.F. Berger, J. Solid State Chem. 153 (2000) 205.
[24] C.M. Varma, Phys. Rev. B 54 (1996) 7328.
[25] A. Yamamoto, K. Oda, J. Phys.: Condens. Matter 14 (2002) 1075.
[26] D. Chowdhury, Spin Glasses and Other Frustrated Systems, World Scientific, Singapore, 1986.
[27] N. Belous, I. Zorin, N. Kulich, I. Lezhnenko, A. Tovstolytkin, Sov. Phys.-Solid State 32 (1990) 887.
[28] E. Lähderanta, K. Eftimova, R. Laiho, H.Al. Kanani, J.G. Booth, J. Magn. Magn. Mater. 130 (1994) 23.
[29] H.E. Stanley, Introduction to Phase Transitions and Critical Phenomena, Clarendon, Oxford, 1971.
[30] A. Moreo, M. Mayr, A. Feiguin, S. Yunoki, E. Dagotto, Phys. Rev. Lett. 84 (2000) 5568.
[31] S. Kirkpatrick, Rev. Mod. Phys. 45 (1973) 574.

[32] M. Mayr, A. Moreo, J. Verges, J. Arispe, A. Feiguin, E. Dagotto, Phys. Rev. Lett. 86 (2000) 135.
[33] L.M. Rodriguez-Martinez, J.P. Attfield, Phys. Rev. B 54 (1996) R15 622.
[34] V. Markovich, G. Jung, Y. Yuzhelevski, G. Gorodetsky, A. Szewczyk, M. Gutowska, D.A. Shulyatev, Ya.M. Mukovskii, Phys. Rev. B 70 (2004) 064414.
[35] J.C. Le Guillou, J. Zinn-Justin, Phys. Rev. Lett. 39 (1977) 95.
[36] J. Mira, J. Rivas, M. Vazques, J.M. Garcia-Beneyetz, J. Arcas, R.D. Sanchez, M.A. Senaris-Rodriguez, Phys. Rev. B 59 (1999) 123.
[37] J.H. Zhao, T. Song, H.P. Kunkel, X.Z. Zhou, R.M. Roshko, G. Williams, J. Phys.: Condens. Matter 12 (2000) 6903.
[38] C.S. Hong, W.S. Kim, N.H. Hur, Phys. Rev. B 63 (2001) 092504.
[39] B.I. Shklovskii, A.L. Efros, Electronic Properties of Doped Semiconductors, Springer, Berlin, 1984.
[40] M.F. Sykes, J.W. Essam, Phys. Rev. 133 (1964) 310.
[41] A.G. Dunn, J.W. Essam, D.S. Ritchie, J. Phys. C 8 (1975) 4219.
[42] S. Kirkpatrick, Phys. Rev. Lett. 36 (1976) 69.
[43] M. Hennion, F. Moussa, G. Biotteau, J. Rodriguez-Carvajal, L. Piusard, A. Revcolevschi, Phys. Rev. Lett. 81 (1998) 1957.
[44] V. Chechersky, A. Nath, I. Isaac, J.P. Franck, K. Ghosh, H. Ju, R.L. Greene, Phys. Rev. B 59 (1999) 497.
[45] H. Huhtinen, R. Laiho, E. Lähderanta, J. Salminen, K.G. Lisunov, V.S. Zakhvalinskii, J. Appl. Phys. 91 (2002) 7944.
[46] R. Laiho, K.G. Lisunov, E. Lähderanta, J. Salminen, V.S. Zakhvalinskii, J. Magn. Magn. Mater. 250 (2002) 267.
[47] S.-W. Cheong, H. Hwang, in: Y. Tokura (Ed.), Colossal Magnetoresistive Oxides, Gordon and Breach, Amsterdam, 2000, p. 237.